Geometrical Dependence of Thermally Excited Mag-Noise Spatial Distribution in Magnetic Tunnel Junction Sensors

T. Zeng[1], Y. Zhou[2], K. W. Lin[3], P. T. Lai[1], and P. W. T. Pong[1]

[1]Department of Electrical and Electronic Engineering, The University of Hong Kong, Hong Kong
[2]Department of Physics, The University of Hong Kong, Hong Kong
[3]Department of Materials Science and Engineering, National Chung Hsing University, Taiwan

The relation between the spatial distribution of thermally excited mag-noise and the geometry of magnetic tunnel junction (MTJ) sensors was studied by micromagnetic simulation. The thermally excited mag-noise in MTJ sensors with rectangular cross section is found to exhibit a spatial distribution in which the tendency could be described as edge effect. The level of this edge effect changes with the aspect ratio of the free layer. As the aspect ratio increases from 0.6 to 1.4, the edge effect is suppressed linearly by nearly two times. This is ascribed to the change of the stiffness field in the free layer. On the other hand, the edge effect is not applicable for MTJ sensors with circular cross section. The central regions of the circular MTJ sensors are the main contributor of the mag-noise. These findings further our understanding on mag-noise behavior in MTJ sensors, and they are useful for suppressing noise in sensor design.

***Index Terms*—Aspect ratio, edge effect, magnetic tunnel junction, spatial distribution, thermal mag-noise.**

I. Introduction

THE ever-increasing magnetic recording density has motivated more and more performance exploration of magnetic tunnel junction (MTJ) sensors recently, in particular, the noise study in nanometer dimension. It has already been demonstrated that the mag-noise, resulting from the thermal magnetization fluctuation, is dominant compared to Johnson and shot noise for sensor size near 100 nm [1]. The thermal mag-noise contains important information about the stability of the sensors. Investigating the thermal mag-noise is essential for MTJ based magnetic sensors. Recently, research in thermal mag-noise spatial distribution led to an in-depth understanding of the origin of the thermal mag-noise from a geometry point of view [2].

In experimental measurements, the noise is extracted from the whole MTJ multi-layer sensor. It is shown that in the current-perpendicular-to-plane (CPP) MTJ sensors, the total mag-noise is a superposition of mag-noise generated by free layer, reference layer, and pinned layer since the motion of the composite pinned and reference layer is essentially uncorrelated with the motion of the free layer [3]. As such, it is not experimentally possible to separately measure the local mag-noise at a specific spatial position on a certain layer. Through micromagnetic simulation, this obstacle can be overcome. The thermal mag-noise from a certain region at one of the layers can be simulated and analyzed.

Mag-noise is not only determined by the volume of the free layer, but also by the overall sensor geometry. In this paper, the relation between the sensor geometry and the mag-noise spatial distribution is thoroughly studied in both rectangular and circular MTJ sensors. The mechanisms related to their distributions are revealed. This study also provides possible ways for reducing the mag-noise from a basic physical viewpoint.

Manuscript received November 05, 2012; revised December 29, 2012; accepted January 20, 2013. Date of current version July 15, 2013. Corresponding author: P. W. T. Pong (e-mail: ppong@eee.hku.hk).

Color versions of one or more of the figures in this paper are available online at http://ieeexplore.ieee.org.

Digital Object Identifier 10.1109/TMAG.2013.2243416

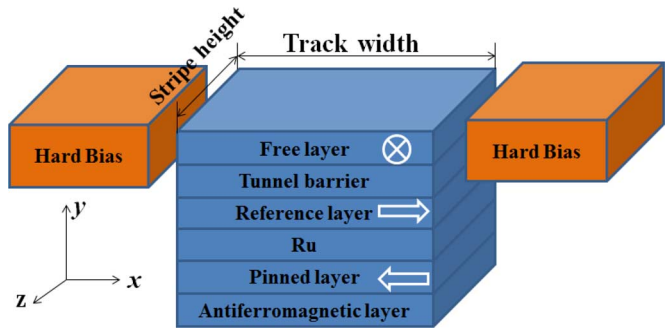

Fig. 1. Three-dimensional illustration of the current-perpendicular-to-plane (CPP) MTJ sensor geometry. The hard bias is utilized to stabilize the free layer magnetization. The hard bias field is along the x-axis while the applied field is along the z-axis. The arrows in reference layer and pinned layer indicate their magnetization orientations while the cross in free layer signifies its magnetization orientation is perpendicular to those of reference layer and pinned layer.

II. Micromagnetic Model for MTJ Sensors

A three-dimensional CPP MTJ sensor structure composed of free layer (FL 5 nm)/tunnel barrier (0.9 nm)/reference layer (RL 2.5 nm)/Ru (1 nm)/pinned layer (PL 2.6 nm)/antiferromagnetic layer (AFM) is modeled as shown in Fig. 1. The saturated magnetization for FL, RL and PL are 8.6×10^5 A/m, 1.4×10^5 A/m, and 1.4×10^5 A/m respectively. The Landau-Liftshitz-Gilbert (LLG) equation is solved utilizing object oriented micromagnetic framework (OOMMF) [4]. The stochastic thermal fluctuation field is assumed to be a Gaussian random process [5] with temperature set as $\mathrm{T} = 60°\mathrm{C}$. The hard bias (HB) field is provided by a fixed uniform external field along the x-axis direction while the applied field is along the z-axis direction. Mesh size is set as 5 nm $\times$ 5 nm$\times$ film thickness. Since the simulation results show that the contribution of thermal mag-noise from the RL and PL are very small compared to the FL, the following analysis is based on only the contribution from the FL.

III. Mag-Noise for MTJ Sensors With Rectangular Cross Section

To explore the geometrical dependence of the thermally excited mag-noise spatial distribution, the FL is divided into seven

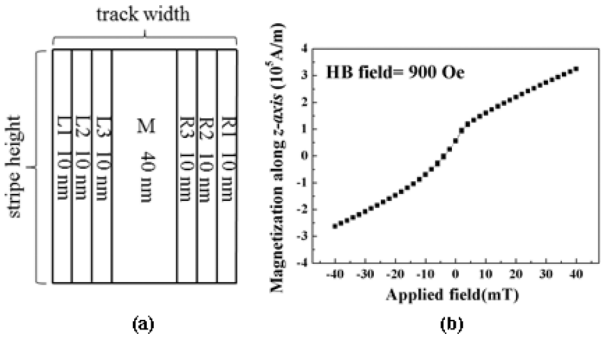

Fig. 2. (a) Free layer is divided into seven rectangular regions denoted as L1, L2, L3, M, R3, and R1 (from left to right) respectively. (b) FL transfer curve when sensor dimension is at 100 nm * 100 nm.

regions along the x-axis direction with each region denoted as L1, L2, L3, M, R3, R2 and R1 respectively as shown in Fig. 2. The L1 and R1 are defined as the edges of the FL. The power spectrum density of each region in the FL is generated by fast Fourier transforming (FFT) of the time-dependent magnetization. The size of the rectangular MTJ is set with track width $(\mathrm{TW}) = 100$ nm and stripe height (SH) ranges from 60 nm to 140 nm. Thus the aspect ratio (SH/TW) ranging from 0.6 to 1.4 can be obtained. The magnetization configurations are obtained for sufficiently long time (10^{-7} sec) and collected every 10^{-11} sec.

A. Noise Spectra of Different Regions in the Free Layer

Based on the FL transfer curves as demonstrated in Fig. 2(b), the HB field and applied field are kept at 900 Oe and 0 Oe, respectively, such that the maximum sensitivity of the MTJ sensor in our model is obtained. The normalized power spectrum densities (PSDs) of the seven regions are calculated for FL aspect ratio value of 0.6, 0.8, 1.0, 1.2 and 1.4 respectively. The PSDs with aspect ratio value 0.6 (Fig. 3) and 1.2 (Fig. 4) are simulated. In Fig. 3 where the aspect ratio is 0.6, the edge regions (L1 and R1) behave actively at low frequency. A reduction in the PSD is observed at 0–1 GHz with the PSD exhibiting a trend of $(1/f)^{\gamma}$, where γ is a number of order unity [6]. This tendency in the edges has been attributed to jumps in the FL magnetization between two or more metastable states [7]. The peaks at 3.3 GHz are also observed in L1, L2, R2, and R1 while the peaks are with relatively large amplitudes in L1 and R1 compared to L2 and R2. No low-frequency features are found in L3, M, and R3. At the middle frequency, the edge regions (L1 and R1) do not behave actively while the L2, L3, M, R3, and R2 regions all exhibit ferromagnetic resonance (FMR) peaks. L2 and R2 regions exhibit the FMR peak at 9.6 GHz, while L3 and R3 regions exhibit the FMR peak at 10.2 GHz. The FMR peak in M is located at 11.3 GHz. In Fig. 4 where the aspect ratio is 1.2, the $(1/f)^{\gamma}$ tendency of PSD is suppressed in the edge regions at low frequency. Instead, peaks at 0.6 GHz are observed in L1, L2 and 0.9 GHz peaks are observed in R1, R2. Similarly, no low-frequency features are found in L3, M, and R3. Meanwhile, FMR-induced middle frequency peaks are also exhibited at the middle frequencies in L2, L3, M, R3, and R2. L2 and R2 regions

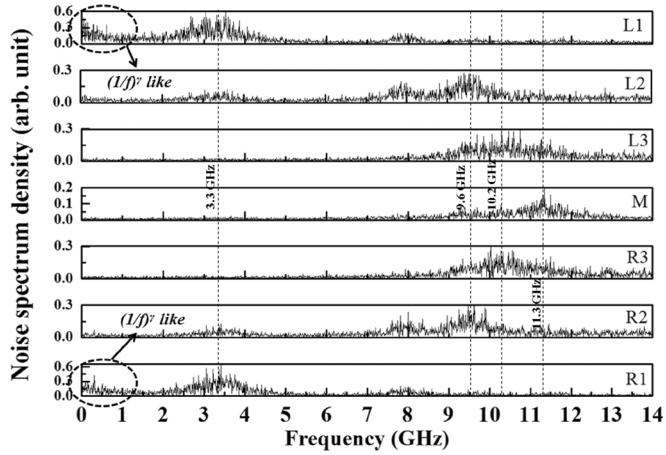

Fig. 3. Simulated thermal mag-noise PSDs of different regions in free layer with aspect ratio 0.6.

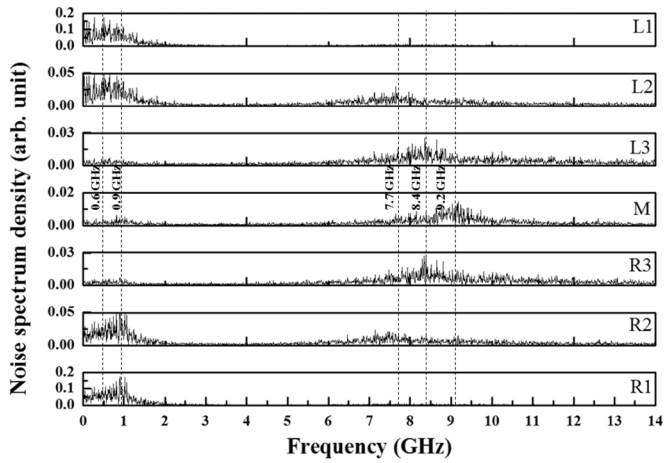

Fig. 4. Simulated thermal mag-noise PSDs of different regions in the free layer with the aspect ratio 1.2.

share the same peak at 7.7 GHz, while L3 and R3 share the same peak at 8.4 GHz. The FMR peak in M is located at 9.2 GHz.

From Figs. 3 and 4, it is obvious that the FL with aspect ratio 0.6 shows FMR peaks at relatively higher frequency than those with aspect ratio 1.2. It can be explained that with the increase of stripe height, the competition between the HB field and the shape anisotropy is changed. The HB field is along the *x-axis*, and the shape anisotropy is also along the *x-axis* for small stripe height. When the stripe height varies from 60 nm to 140 nm, the shape anisotropy along the *x-axis* is reduced, which results in the reduction of effective stiffness along the *x-axis*. Since the FMR peak scales approximately with the square-root of the stiffness field [2], the increase of the aspect ratio of the FL leads to the decrease of effective stiffness field which shifts the position of the FMR peaks to lower frequencies.

B. Size Dependence of the Edge Effect

In order to study the influence of the aspect ratio on the mag-noise spatial distribution, the mag-noise PSDs are integrated from 0–4 GHz in each of the seven regions with various aspect ratios.

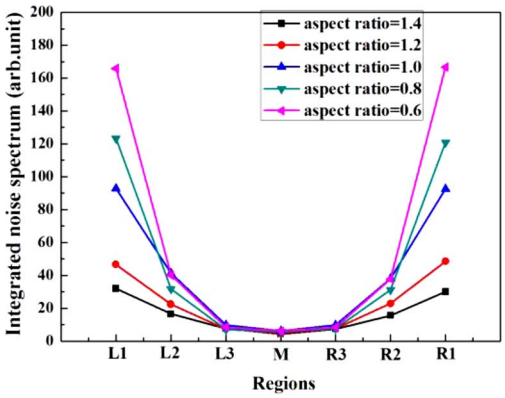

Fig. 5. Integrated thermal mag-noise in the range of 0–4 GHz versus different regions with various aspect ratios.

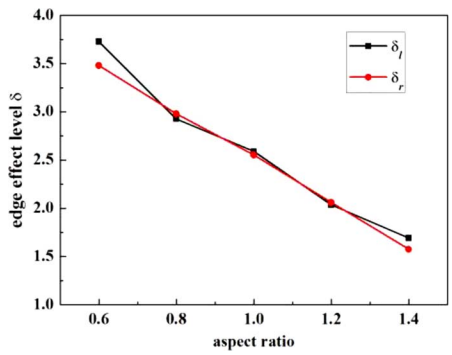

Fig. 6. Edge-effect level versus free-layer aspect ratios.

The relation between the integrated low-frequency mag-noise and the spatial location with various FL aspect ratios is computed and shown in Fig. 5. There exists low-frequency mag-noise distribution gradient from the edges to the middle under various aspect ratios. The edges are the main contributor of thermal mag-noise in FL even under different aspect ratios. This edge effect phenomenon can be explained by multi-domain formation in FL as explained in [2]. Fig. 6 is provided to further explore the relation between the aspect ratio and the edge effect. To quantity the edge effect, we define the edge-effect level δ in the following equations:

$$\delta_l = \frac{\mathrm{S_{L1}} - \mathrm{S_{L2}}}{\mathrm{S_{L2}}} \tag{1}$$

$$\delta_\mathrm{r} = \frac{\mathrm{S_{R1}} - \mathrm{S_{R2}}}{\mathrm{S_{R2}}} \tag{2}$$

where δ_l and δ_r represent the edge effect level in the left-edge region and right-edge region respectively; $\mathrm{S_{L1}}, \mathrm{S_{L2}}, \mathrm{S_{R1}}$, and $\mathrm{S_{R2}}$ are the integrated low-frequency mag-noise in L1, L2, R1, and R2 regions respectively. As can be seen from Fig. 6, δ_l and δ_r change with the aspect ratio in a similar trend. It is obvious that the mag-noise decrease rate for the left-edge region and the right-edge region mostly agree with each other. There are only slight difference between δ_l and δ_r when the aspect ratio was at 0.6 and 1.4. Since the parameters δ_l and δ_r exhibit nearly the same trend with the aspect ratio, it is demonstrated that the edge effect maintains good spatial geometric symmetry. The aspect ratio does not change the spatial geometric symmetry of edge effect. The trends in the Fig. 6 are modeled with linear equations:

$$\delta_l = k_l \cdot a + l_l \tag{3}$$

$$\delta_r = k_r \cdot a + l_r \tag{4}$$

where k_l and k_r stand for the line slopes in Fig. 6, l_l and l_r are the corresponding intercepts, and a is the aspect ratio. It is calculated that $k_l = -2.76, k_r = -2.47, l_l = 5.35$, and $l_r = 4.96$. From (3) and (4), it is obtained that the edge-effect level decreases with the aspect ratio. The decrease of the edge effect level induces the suppression of the edge effect in the FL, which leads to a relatively uniform spatial distribution of thermal low-frequency mag-noise. Considering that the edge regions are the main contributor of mag-noise in rectangular FL [3], increasing the aspect ratio is very favorable for the sensor design since the suppression of edge effect in FL leads to the decrease of the total mag-noise in FL.

The above phenomenon can also be explained by the stiffness field distribution in the FL. Since there is a strong correlation between the shape anisotropy and the effective stiffness field in the FL, the variation of the aspect ratio consequently changes the stiffness field in the FL. Small aspect ratio and thus large stiffness field in edges leads to a more prompt spin tilting around the edges while large aspect ratio results in a more reluctant spin tilting around the edges. The stiffness field spatial distribution will be demonstrated in future study.

Equations (3) and (4) can predict the edge-effect level as the aspect ratio of the MTJ sample changes. It should be noted that the applicable scope of (3) and (4) is under the assumption that the TW maintains at 100 nm and the sample is rectangular with aspect ratio range of 0.6–1.4. Too small or too large aspect ratio will result in nanowire-like sample, which is not considered here.

IV. Mag-Noise for MTJ Sensors With Circular Cross Section

The mag-noise simulation and analysis are extended to MTJs with a circular cross section. The radius is set as 100 nm. The circular MTJ is divided into four regions with identical area denoted as I, II, III, and IV as shown in Fig. 7(a). Thus the widths of the ring-shape regions I, II, and III are 13.4 nm, 15.9 nm and 20.1 nm respectively. The central circular region IV is with radius 50 nm. Using the same simulation parameters as the MTJ sensor with rectangular cross section, the PSDs for these four regions are computed in Fig. 7(b). At low frequency, the edge regions (I and II) do not behave actively while there is slightly larger PSD in region III. For the central region IV, the PSD increases with the frequency. At the middle frequency, peaks are observed in regions I, II, and III at 8.7 GHz, which should be ascribed to the FMR. However, no peaks appear in region IV.

By observing the time-tracing circular domain structure during simulation, it is found the edges are always well pinned under the HB field. No multi-domain structures are formed. However, for the central region IV, some random switching occurs along with the formation of local vortex resulting in the relatively large low-frequency PSD.

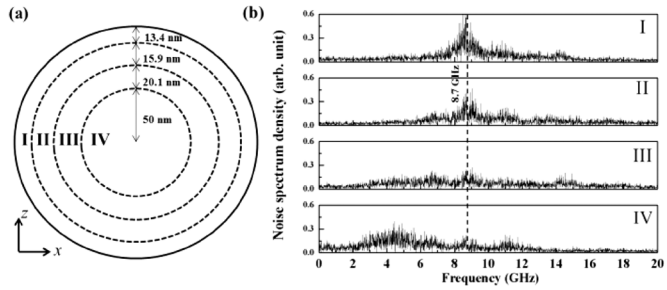

Fig. 7. (a) Free layer geometry for MTJ sensor with circular cross section. I, II, III, and IV stands for four regions with identical area. (b) Normalized noise spectrum densities for regions I, II, III, and IV respectively.

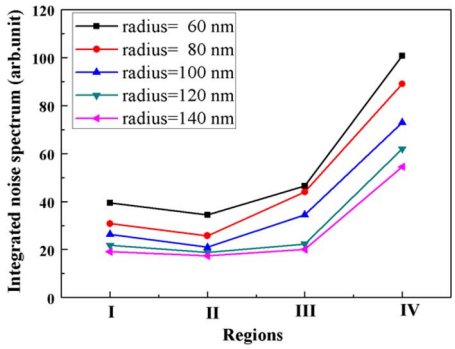

Fig. 8. Simulated thermal mag-noise PSDs of different regions in free layer with the FL radius changes from 60 nm to 140 nm.

To further explore the influence of circular dimension on the mag-noise spatial distribution, the normalized PSDs are integrated from 0 to 4 GHz under various circular radii. The distribution of the integrated noise spectrum for circular FL with different radii is shown in Fig. 8. For edge regions I, II, and III, the integrated mag-noise gradually increases as the radius decreases. At a certain radius, the differences among the integrated mag-noise in I, II, and III are very slight. The edge effect no longer exists in MTJ sensors with circular cross section. On the contrary, the central region IV becomes the main source of the low frequency thermal mag-noise due to the formation of local vortex. This central effect from region IV to region III can also be defined as:

$$\varepsilon = \frac{S_{IV} - S_{III}}{S_{III}} \tag{6}$$

where S_{IV} and S_{III} are the integrated low-frequency mag-noise in region IV and region III respectively. As the radius increases from 60 nm to 140 nm, the value of ε increases from 1.17 to 1.73, as shown in Fig. 9. Therefore, the effect of the local vortex at the center on the low-frequency mag-noise strengthens as the size of the circular sensor becomes larger. The result manifests

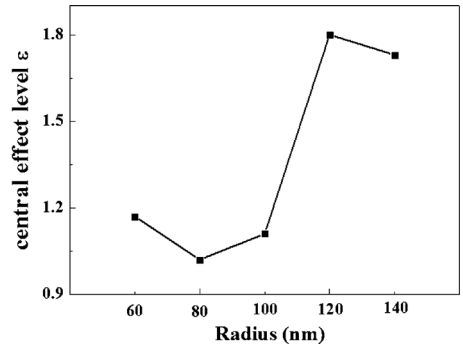

Fig. 9. Relation between central-effect level and free-layer radius.

that the central region is the dominant origin of low-frequency thermal mag-noise in relatively large circular MTJ sensors.

V. Conclusion

We investigated the geometrical dependence of the thermal mag-noise spatial distribution in MTJ sensors via micromagnetic simulation. By integration of the PSDs from 0–4 GHz, it is shown that the increase of the FL aspect ratio results in a linear suppression of edge effect in the FL of rectangular cross section. In MTJ sensors with circular cross section, it is revealed the low-frequency mag-noise origins from central regions in the FL rather than the edge regions. This phenomenon is more dominant for circular sensors with relatively large radius.

Acknowledgment

This work was supported by the Seed Funding Program for Basic research and Small project Fund from the University of Hong Kong, the RGC-GRF under Grant HKU 704911P, the University Grants Council of Hong Kong under Contract AoE/P-04/08, and ITF Tier 3 funding under Grant ITS/112/12.

References

[1] Y. Zhou, A. Roesler, and J.-G. Zhu, "Experimental observations of thermally excited ferromagnetic resonance and mag-noise spectra in spin valve heads," *J. Appl. Phys.*, vol. 91, pp. 7276–7278, 2002.
[2] T. Zeng *et al.*, "Edge effect on thermally excited mag-noise in magnetic tunnel junction sensors," *IEEE Trans. Magn.*, vol. 48, pp. 2831–2834, 2012.
[3] O. Heinonen and C. H. Seok, "Thermal magnetic noise in tunneling readers," *IEEE Trans. Magn.*, vol. 40, pp. 2227–2232, 2004.
[4] M. J. Donahue and D. G. Porter, OOMMF User's Guide [Online]. Available: http://math.nist.gov/oommf
[5] [Online]. Available: http://www.nanoscience.de/group_r/stm-spstm/projects/temperature/download.shtml
[6] W. K. Park *et al.*, "Noise properties of magnetic and nonmagnetic tunnel junctions," *J. Appl. Phys.*, vol. 93, pp. 7020–7022, 2003.
[7] S. Ingvarsson *et al.*, "Low-frequency magnetic noise in micron-scale magnetic tunnel junctions," *Phys. Rev. Lett.* , vol. 85, p. 3289, 2000.